Finite Element Analysis of the Acoustic Behavior of Poroelastic Materials Based on Experimentally Determined Frequency-Dependent Material Properties

P. Schrader[1], F. Duvigneau[2], M. Gavila-Lloret[3], H. Rottengruber[1], U. Gabbert[2]
[1]Otto von Guericke University Magdeburg, Department of Mechanical Engineering, Chair of Energy Conversion Systems of Mobile Applications, Universitätsplatz 2, D-39106, Magdeburg, Germany
[2] Otto von Guericke University Magdeburg, Department Mechanical Engineering, Chair of Numerical Mechanics, Universitätsplatz 2, D-39106, Magdeburg, Germany
[3]BMW Group, Department of Air-Borne-Acoustics, Knorrstraße 147, D-80788, Munich, Germany

e-mail: **peter.schrader@ovgu.de**

Abstract
The paper examines the possibility to predict the noise absorption behavior of poroelastic materials with a simple modeling approach trying to avoid the extensive experimental efforts of advanced modeling strategies based upon the Biot theory of poroelastic media. The concept is to experimentally determine the frequency-dependent stiffness and damping properties in terms of the dynamic complex Young's modulus within the examined frequency range. It is assumed that experimental data of the dynamic stiffness and damping characteristics can capture all dissipative influences, which are normally estimated by extended Biot models. Besides avoiding the requirement to determine the poroelastic parameters, the numerical effort is reduced, as it is no longer a coupled problem and the number of degrees of freedom is decreased as well. The results of the approach show high compliance with the numerical results of synchronous Biot modeling for the same application case. The application of the simplified approach is limited by the highest reliable frequency of the experimental measurement of the dynamic Young's modulus and damping ratio, which actually reaches 2 kHz if no extrapolation is desired. Parallel to the simulation, acoustic measurements with 19 different poroelastic materials were conducted in an anechoic room to obtain a database for the validation of the simulation results and to get an overview of the possible acoustic behavior of different simple plastic foams. The results show coincidence with the experimentally determined dynamic Young's modulus, pore size and density of the material.

1 State of the art in numerical modeling of poroelastic media

The theory of poroelasticity by Biot-Allard [1–3] is the most extended approach to describe the sound propagation in elastic porous media. Its main underlying assumption is the homogenization. This means that, provided that the wavelengths of the waves propagating inside the material are much larger than the pores size, the biphasic aggregate can be considered as a homogenous medium in which the two phases are simultaneously present. Consequently, the resolution of the pores on the microscale is avoided. The two governing equations have the form of a fluid-structure interaction problem with the particularity that the mechanical coupling between the elastic frame deformation and the fluid behavior is not limited to the fluid structure interfaces, but is of a volume nature.

The parameters defining the equations coefficients can be grouped into three classes: fluid, elastic and poro-mechanical. The first set includes the material properties of the filling fluid, namely its density ρ_0, its viscosity η_0 and the speed of sound c_0. The elastic parameters characterize the response of the frame in vacuum and are typically the Young's modulus E, the Poisson's ratio ν, the structural damping coefficient η and the density of the drained material ρ_1. The poro-mechanical parameters help to link the microscopic

thermal and viscous effects at a local level with the changes in the macroscopic effective bulk modulus and effective dynamic density. This requires a constitutive model as, for example, the one proposed by Johnson-Champoux-Allard (JCA,[4], [5]), which is employed as reference in this paper.

Some of the procedures to determine the values of these mentioned material parameters can be found in [6-8]. The characterization of poroelastic materials is associated with inaccuracies of different kind. First, the tested samples often include inhomogeneities as a result of the manufacturing processes. Second, the measurement equipment and techniques employed suffer from reproducibility issues as highlighted in [9]. Lastly, the use of elastic properties obtained from quasi-static tests is a common practice, but their value may differ significantly at higher frequencies [10]. Thus, a frequency-dependent testing of the elastic properties may be considered as a proper modeling approach. In Section 2 below, a measurement technique for this purpose is introduced.

The key for a correct prediction of the acoustic effects in poroelastic material is the proper modeling of its dissipation effects. They are subdivided into structural damping losses W_{str}, viscous losses W_{visc} and thermal effects W_{th}. For the displacement-pressure (u, p)-formulation of the Biot theory [8] explicit relations for these losses are derived in [11]. The total losses are obtained by integration over the material domain Ω. The structural damping loss W_{str} is determined as the Frobenius inner product of the imaginary part of the complex stress tensor of the elastic solid in vacuum $\Im\left(\underline{\underline{\hat{\sigma}}}^{s}(\mathbf{u})\right)$ and of the strain tensor $\varepsilon(\mathbf{u}^*)$ of the complex conjugate deformations $\mathbf{u}^*$ of the solid phase

$$W_{str} = \int_{\Omega} \Im\left(\underline{\underline{\hat{\sigma}}}^{s}(\mathbf{u})\right) : \varepsilon(\mathbf{u}^*) d\Omega . \tag{1}$$

The viscous losses W_{visc} consist of the losses in the solid phase W_{visc}^{s}, the fluid phase W_{visc}^{f} and due to the coupling between solid and fluid phase W_{visc}^{sf} as

$$W_{visc} = W_{visc}^{s} + W_{visc}^{f} + W_{visc}^{sf} . \tag{2}$$

They are calculated as

$$W_{visc}^{s} = -\pi\omega^2 \int_{\Omega} \Im(\tilde{\rho}) \cdot |\mathbf{u}|^2 d\Omega \tag{3}$$

and

$$W_{visc}^{f} = \pi \int_{\Omega} \Im\left(\frac{\phi^2}{\tilde{\rho}_{22}\omega^2} \right) \cdot |\nabla \mathbf{p}|^2 d\Omega \tag{4}$$

and

$$W_{visc}^{sf} = -2\pi \int_{\Omega} \Im\left(\frac{\phi}{\tilde{\alpha}} \right) \cdot \Re\left(\mathbf{u}^* \nabla p\right) d\Omega . \tag{5}$$

In these equations ϕ denotes the open porosity. The tilde symbol indicates that the corresponding material coefficient is complex and frequency-dependent, namely the effective density $\tilde{\rho}$, the mass coefficient for the fluid phase $\tilde{\rho}_{22}$ and the dynamic tortuosity $\tilde{\alpha}$. Their calculation in the context of the theory developed by Johnson [4] requires the experimentally determined open porosity ϕ, the airflow resistivity σ, the tortuosity α_∞ and the viscous characteristic length Λ. Finally, the thermal dissipation losses are given by the relation

$$W_{th} = \frac{\phi \cdot \pi \cdot \Re\left(\tilde{R}\right)}{\left|\tilde{R}\right|^2} \int_{\Omega} |p|^2 d\Omega \tag{6}$$

that furthermore requires the real part of the complex elastic coefficient of the fluid phase $\Re\left(\tilde{R}\right)$. If the stiffness of the solid phase is much larger than that of the bulk material and of the filling fluid, its value can be approximated by $\tilde{R} = \phi \cdot \tilde{K}_f$ using the open porosity and the dynamic bulk modulus of the air in the pores $\tilde{K}_f$. The dynamic bulk modulus has to be calculated from the experimental parameters

mentioned above as well as from the thermal characteristic length Λ', the adiabatic index, the static pressure and the Prandtl number. Their relation is derived by Champoux and Allard in [5].

The model briefly sketched above is the state of the art in the modeling of poroelastic materials. It is based upon extensive and highly advanced measurements for each poroelastic material specimen that have to be carried out by specialized institutions. The advantage of the model is its ability to estimate the contributions of the different dissipation mechanisms. Since the losses described in Eqs. (1-6) cannot or can only partially be separated in experiments (e. g. by avoiding fluid damping, solid-fluid interaction and thermal dissipation by evacuation of the open-cell porous material) such modeling enables to gain more knowledge about the partition of each mechanism in overall damping. The model allows a separate investigation of a rigid frame model and a limp frame model of the porous structure and thus the separation of fluid and solid-fluid interaction effects (stiff frame) from solid effects (elastic frame).

2 Simplified approach using experimentally determined damping parameters

The assumption is that the sum of the effects of all poro-mechanical parameters of a given material can effectively be measured and summarized by the frequency-dependent complex Young's modulus in the frequency range of interest. This avoids the experimental efforts and the error sources described in the section above. This approach will not allow an estimation of the contribution of each damping mechanism to the overall dissipation, but a frequency-dependent characterization of the overall dissipation whose single contributions are summarized in a simple expression as Eq. (1). This leads to a numerical solution based on the principle of virtual displacements for homogenous materials with linear elastic material behavior using only one damping term. Transformed in the frequency range, it results in the following linear differential equation system

$$(-\omega^2\mathbf{M} + i\omega\mathbf{C} + \mathbf{K})\tilde{\mathbf{u}} = \tilde{\mathbf{f}}\,, \tag{7}$$

wherein $\mathbf{M}$, $\mathbf{C}$, and $\mathbf{K}$ represent the system mass matrix, the system damping matrix and the stiffness matrix. The vector of the complex external forces $\tilde{\mathbf{f}}$ is derived from a force signal in the time domain by discrete or fast Fourier transform (DFT / FFT) and thus depends on the system's angular excitation frequency ω. The displacements $\tilde{\mathbf{u}}$ are thus complex and frequency-dependent as well. In the approach that is pursued in this paper the damping matrix $\mathbf{C}$ and the stiffness matrix $\mathbf{K}$ are frequency-dependent and contain expressions of the experimentally determined, frequency-dependent dynamic Young's modulus E and the dynamic damping ratio D. The Poisson's ratio ν is assumed to be constant. Hence, the approach results in a significant reduction of material parameters to be measured or estimated in advance. In this approach a successful prediction mainly depends on the appropriate measurement of the complex Young's modulus in the frequency range of interest. The coupled vibroacoustic models introduced in the fourth section will be used for the acoustical prediction based on the proposed simplified elastic approach. The required material characterization is described in the following Section.

2.1 Experimental damping measurements

The experimental setup used for the characterization of the frequency-dependent stiffness and damping properties of the investigated foam materials is shown in Figure 1. A material sample of a thickness of 20 mm and a diameter of 30 mm was placed between an electrodynamic shaker and a seismic mass. The shaker excited the material sample with an harmonic oscillation.

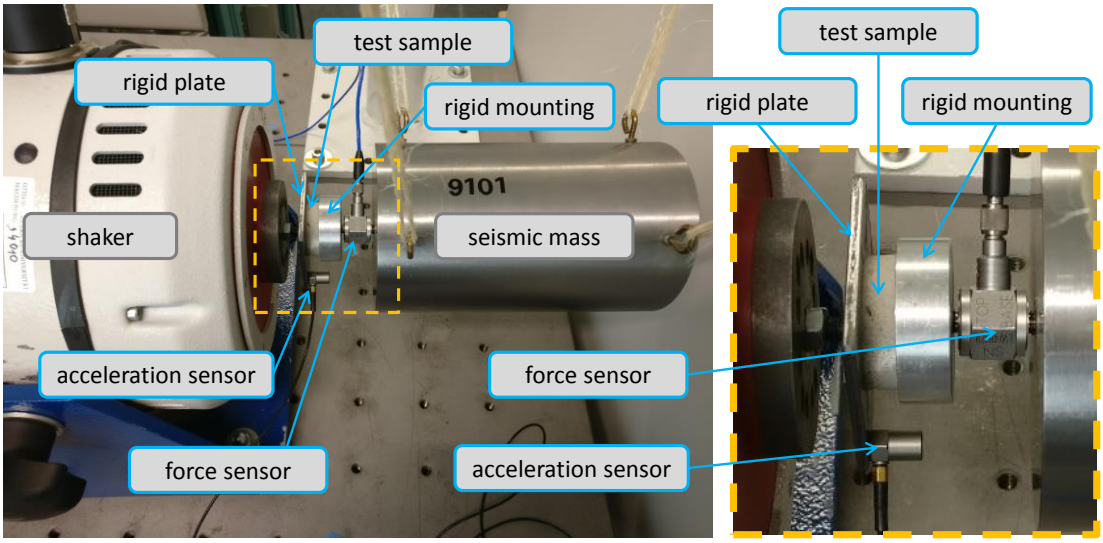

Figure 1: Experimental setup for determining the frequency-dependent properties of damping materials

Except for the material sample of interest, the whole setup is assumed to be rigid. Hence, the system can be treated as a single degree of freedom spring-mass-damper system. The mounting on a seismic mass under free-free boundary conditions (eigenfrequencies almost zero) was used to avoid resonances of the mounting part within the frequency range of interest. Each frequency was excited by a monofrequent harmonic force with the help of an electrodynamic shaker and measured separately. The measured data include the excitation force (force sensor) and the displacement (acceleration sensor). The retrieved acceleration has to be transformed to obtain the displacement. To avoid errors caused by numerical integration the relation

$$x(t) = \hat{x}e^{-i\omega t} \rightarrow a(t) = \ddot{x}(t) = -\omega^2 \hat{x}e^{-i\omega t} \rightarrow a(t) = -\omega^2 x(t) \tag{8}$$

was used, which holds for harmonic states. The resulting Young's modulus was determined out of the spring stiffness under consideration of the dimensions of the test sample. The spring stiffness was calculated with the help of the measured force and displacement. Moreover, the damping properties, either expressed as the loss modulus E'', the loss factor $\eta = E''/E'$ or the damping ratio D, were obtained from the hysteresis loss in the force-displacement diagram. These calculations were repeated at each measured frequency in the investigated range beginning at 0.1 kHz and increased with a constant step size of 0.1 kHz. The maximum operable frequency was limited by the power of the shaker. Furthermore, it is important that the signal to noise ratio is feasible and that resonance effects as well as other perturbations were avoided. With the presented setup it was possible to reliably determine the material parameters up to 2 kHz. Several characterization methods and influence parameters and how they affect the resulting frequency-dependent material properties were investigated in advance. Additionally, numerous numerical studies were also conducted to gain a better understanding of the working principle of the setup and all important influence parameters. More detailed information is given in [12].

Figure 2 shows different foams whose dynamic parameters were determined with the test method described above. The equally scaled images display the macroscopic pore structure of different foam materials sorted by their density. Most of the foams are polyesters (PES) and polyethers (PETH). The polyester foams have a very regular porosity, with a small pore size variation within each material and a decreasing pore size with increasing density. The PES 1 foam haptically shows a higher rigidity than the other polyesters with higher density. In comparison to the PES foams, each of the polyether materials show a bigger variance of the pore size and a more irregular, stochastic structure. The pore size decreases with increasing density as well. There are no samples with palpable high rigidity. The melamine resin sample (MR) also has a high variance of the pore sizes and seems to be stiff analogously to the polyethylene foam (PE), which presents very small pores and a regular pore size. The relatively stiff polyurethane foam (PUR) has a small pore size and shows a medium pore size variance. The EPDM foams of high density have a smooth surface and very small, regular pores.

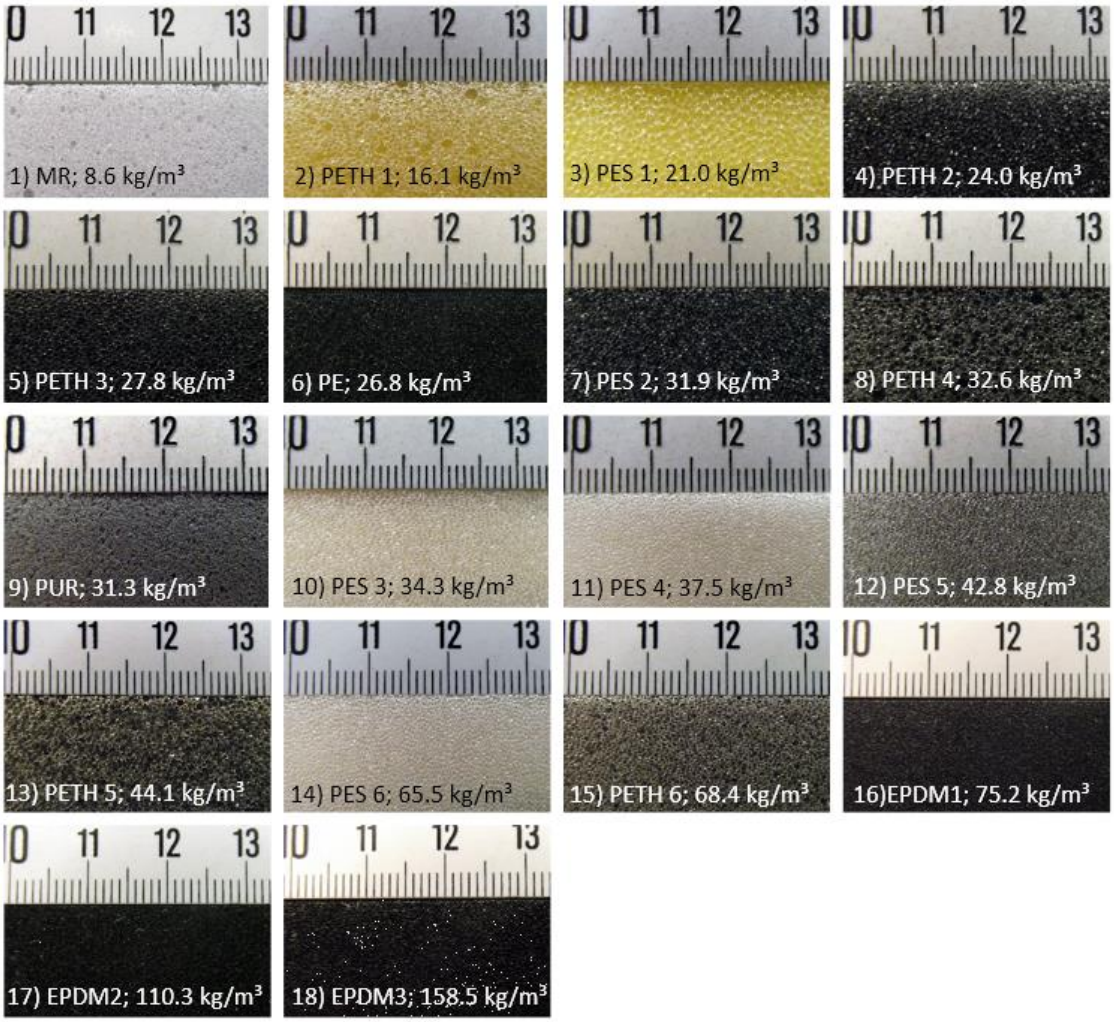

Figure 2: Investigated foams. The abbreviations stand for: EPDM – ethylene propylene diene monomer; MR – melamine resin; PE – polyethylene; PES – polyester; PETH – polyether

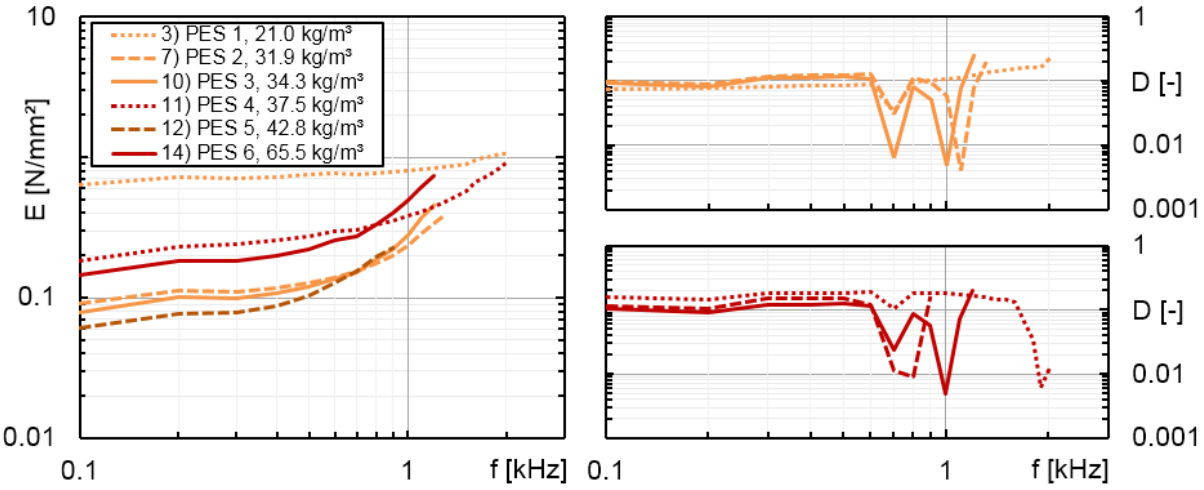

Figure 3: Young's modulus E (left diagram) and damping ratio D (right diagrams) of polyester foams with a thickness of 20 mm

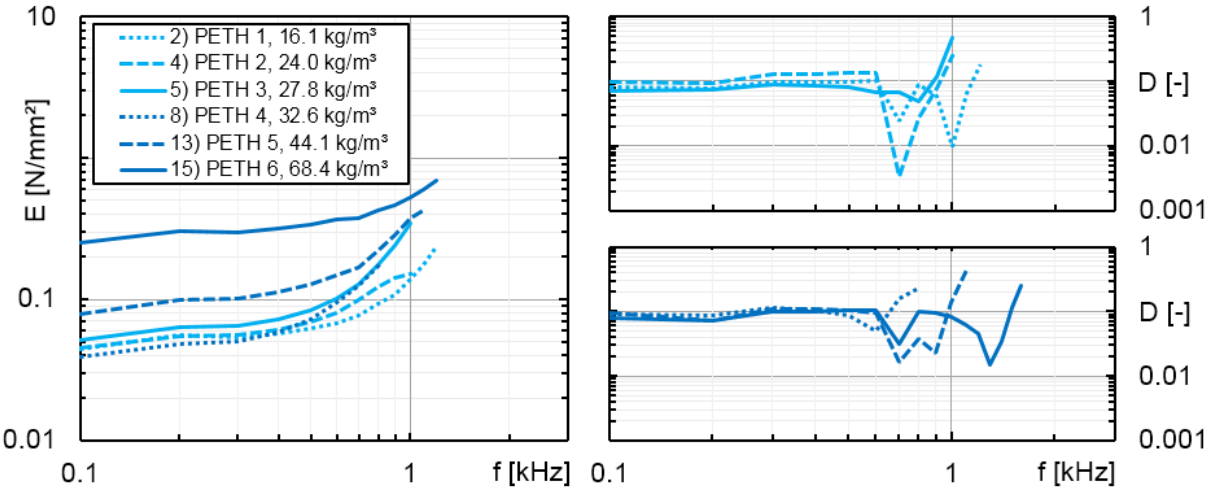

Figure 4: Young's modulus E (left diagram) and damping ratio D (right diagrams) of polyether foams with a thickness of 20 mm

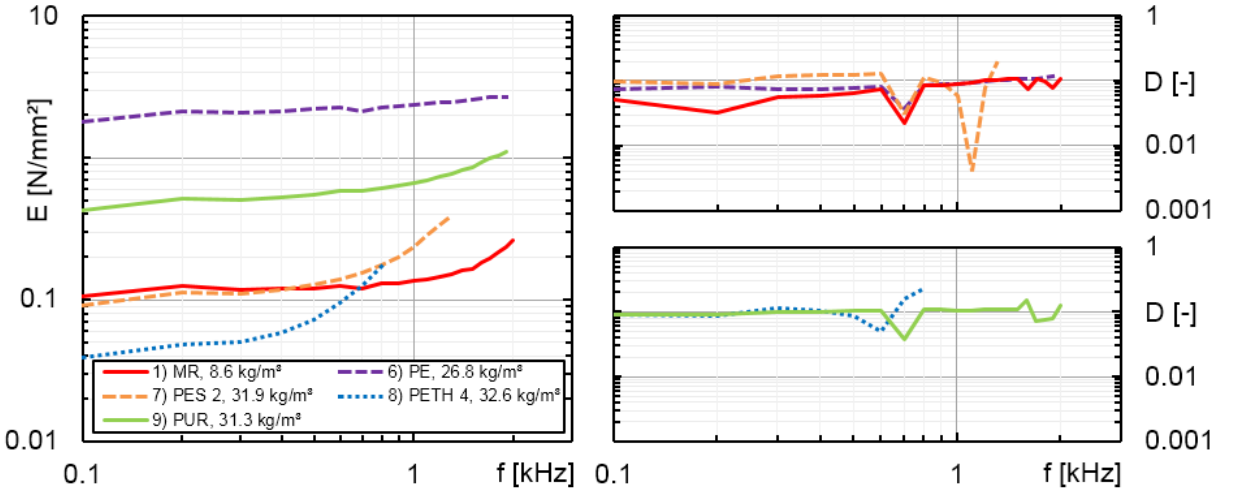

Figure 5: Young's modulus E (left diagram) and damping ratio D (right diagrams) of plastic foams of different materials with a thickness of 20 mm

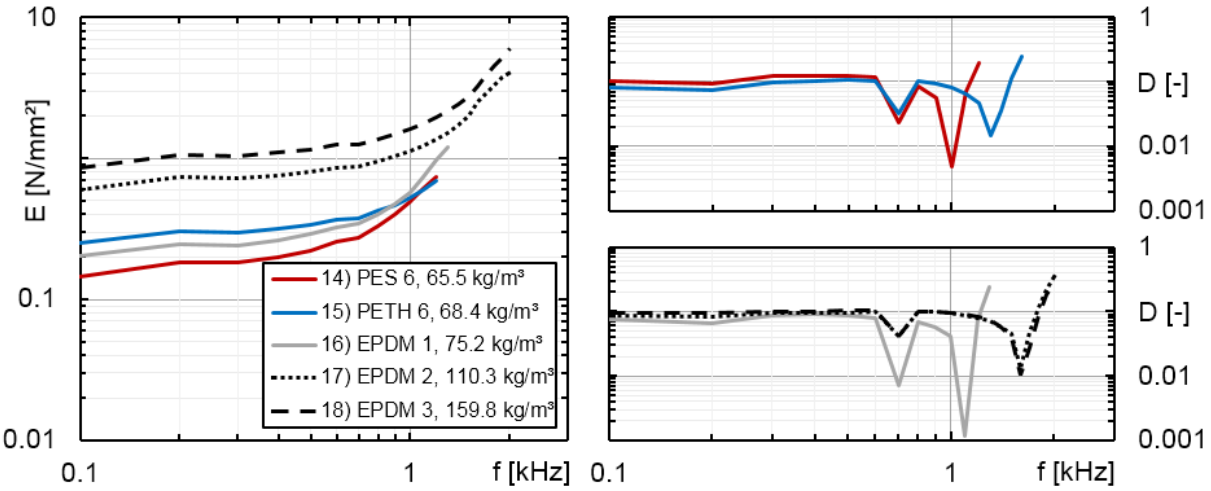

Figure 6: Young's modulus E (left diagram) and damping ratio D (right diagrams) of heavy and EPDM plastic foams with a thickness of 20 mm

The Figures 3-6 show the experimentally determined dynamic Young's modulus E and the dynamic damping ratio D measured with the test setup displayed in Figure 1. The Young's modulus steadily increases with the frequency. The foams with a stiff appearance as MR, PES 1, PE and PUR present, in comparison to the softer foams as PETH 1-5, just a slight increase of the Young's modulus throughout the frequency range. Moreover, their results show small irregularities in the damping ratio. In the case of the PUR foam (Figure 5) the damping could even be assumed to be frequency-independent up to 2 kHz, where it is not determinable anymore. Up to 0.6 kHz all investigated materials show an almost constant damping ratio close to 0.1. Here, a higher Young's modulus causes a higher absolute loss modulus E'' under a constant damping ratio. Above this frequency, many of the investigated materials show a higher slope of the Young's modulus and this increase corresponds with a characteristic local decrease of the damping ratio and of the loss modulus. At this point it cannot be excluded that these local minima are no intrinsic material properties of the specific samples but result from resonant interactions between the experimental setup and the probes. Actually, it must furthermore be stated that the current experimental configuration does not allow to determine the elastic material data for higher audible frequencies.

3 Acoustic measurements

The materials were investigated in an anechoic room with full absorption above 100 Hz at all walls. Figure 7 shows the experimental setup. Each material probe was fixed with a steel frame at the surface of an aluminum plate with the dimensions 400 x 200 x 18 mm. The frame was fixed as shown in the lower right image with screw nuts at thread rods that were screwed into the plate. The screw nuts were tightened at each prototype until the small gap between foam and plate had disappeared at each side. Furthermore, the samples were tested at a steel sheet with identical dimensions but a thickness of 1 mm. Here, the materials were fixed with a double-sided tape. The plate was coupled to an electrodynamic shaker by a rod that was tightly connected with the backside of the plate (lower left image of Figure 7). The shaker was excited with a white noise current generated and amplified with a constant magnitude by a signal

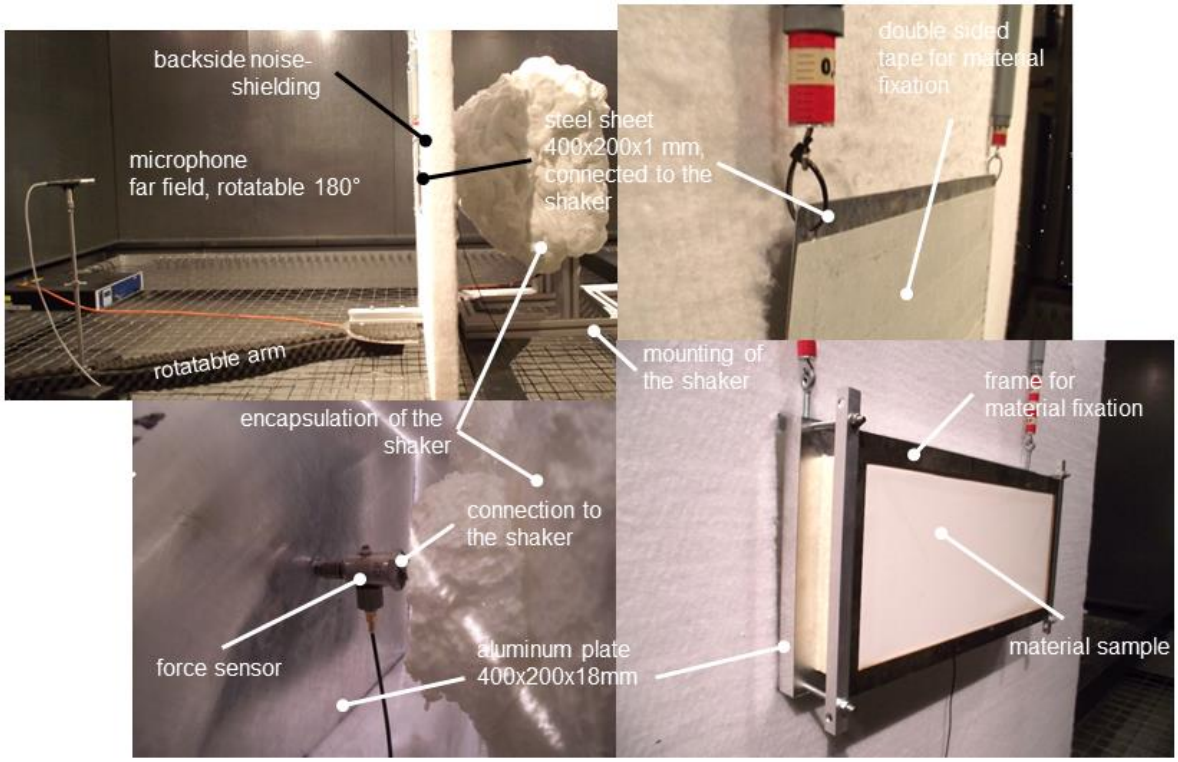

Figure 7: Test setup for acoustic measurements in an anechoic chamber

generator and an amplifier. The transduced force between shaker and plate was measured with a force sensor mounted in line with the connection rod. The radiated noise of the plate was recorded by a single

microphone positioned in a distance of 0.9 m from the plate and in the height of the plate's center. The microphone was rotated horizontally around the plate between 0° and 180° in steps of 10° to obtain a directional characteristic of the sound pressure level (SPL) in the frequency range 0.1-12.8 kHz. This directional characteristic was averaged arithmetically so that the overall SPL characteristic contains all frequency lobes of the sound radiating structure. Within the anechoic room, the averaged SPL represents the radiated power of the plate in the far field. The results are shown below as third octave band levels of the SPL characteristics. The insertion loss (IL) of the foam mounted at the plate was calculated by subtraction of its third octave band SPL from the third octave band SPL of the uncovered plate, which is possible due to the identity of the sound pressure level and the sound power level under free-field-conditions in the far field.

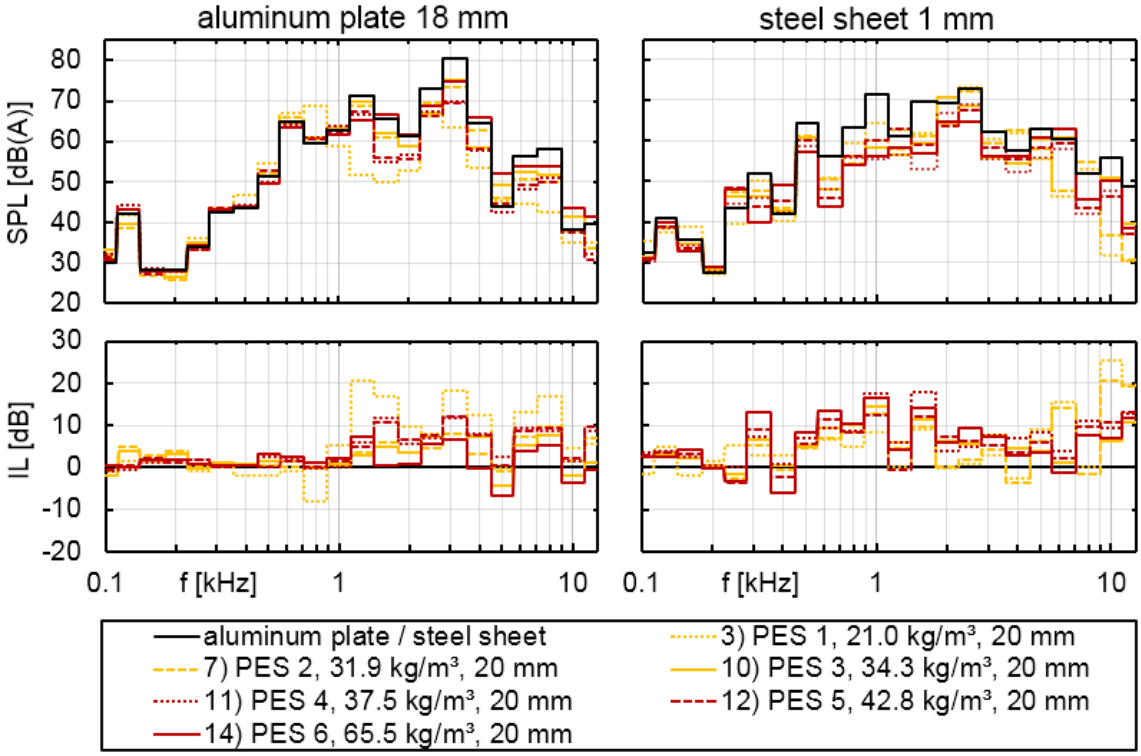

Figure 8: Sound pressure level and insertion loss (IL) of polyester foams of different density

The Figure 8-12 show the sound pressure level and the IL that were measured in the test bench for all of the investigated foams fixed on a 18 mm aluminum plate and on a 1 mm steel sheet. The materials and their appearing order in the Figure 8-11 are identical to the ones shown in the Figure 3-6. The left and right diagrams compare the noise reducing effect measured at the stiff aluminum plate where each foam's influence on the system's stiffness was negligible small, in comparison to the effect on the 1 mm steel sheet, where it was not. The lower stiffness of the steel sheet results in a first structural resonance below 0.3 kHz and in significant noise reductions below 1 kHz for all foams. However, for the thick aluminum plate no significant noise reductions were detected below 1 kHz in any measurement. On the other hand, the effect of a noise reduction due to a stiffening of the structure by a foam is most apparent in the right diagrams of Figure 10. Here, at the 1 mm steel sheet the foam with the highest dynamic Young's modulus at low frequencies, the PE-Foam (violet curve), leads to significant reductions in the low frequency range. For the aluminum plate a comparable effect is not visible.

The acoustic measurements do not show a coincidence with the characteristic damping ratio decrease of soft foams at certain frequencies shown in the Figure 3-6. The specific materials do not show a generally reduced insertion loss in the third octave bands for these frequencies. The foams with the biggest pore size, PES 1 and PETH 1, show a significantly higher noise reduction above 1 kHz on the aluminum plate. The comparison of the IL in the diagrams of Figure 8 and Figure 9 shows a high degree of similarity. It is obvious that the effects of the PES and PETH materials are similar. The changes in the acoustic behavior

due to an increase of the material density are complex, but occur in a synchronous pattern for both materials.

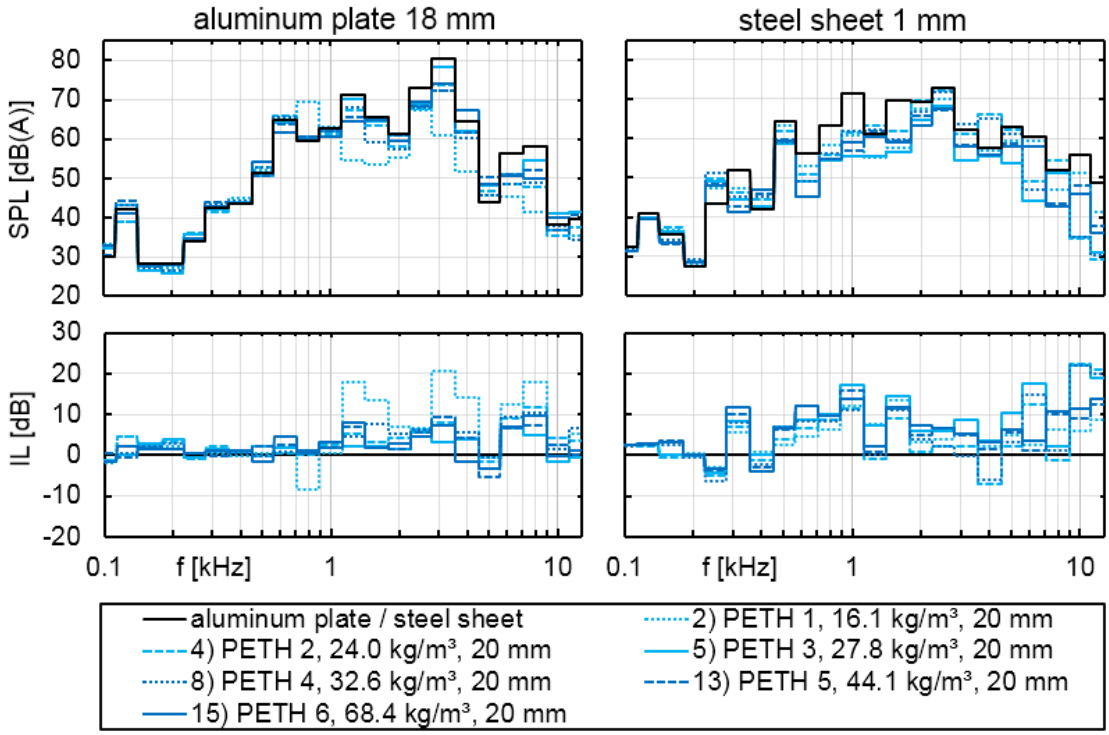

Figure 9: Sound pressure level and insertion loss of polyether foams of different density

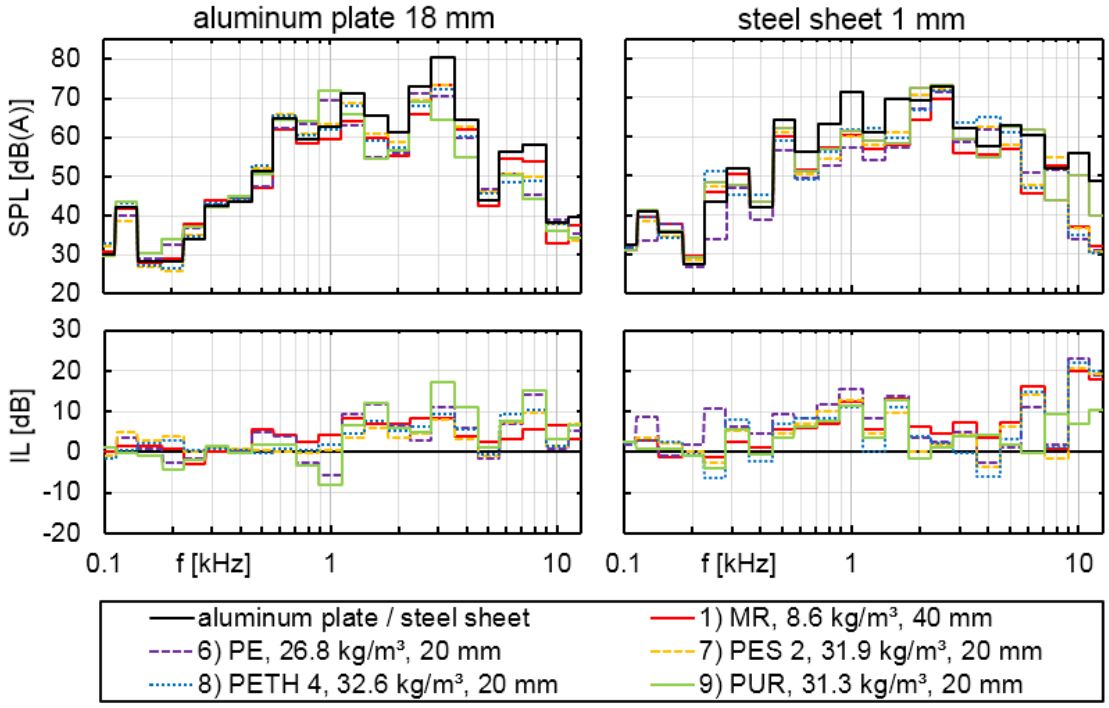

Figure 10: Sound pressure level and insertion loss of foams of different materials

In Figure 10, the effects of different foam materials with various dynamic Young's modulus are presented. The low frequency effect of the PE foam on the steel sheet due to the foam high dynamic stiffness has already been mentioned above. In comparison, the PETH 4 foam with a low dynamic Young's modulus at

low frequencies as well as the MR and the PES 2 foam have no significant influence on the steel sheets noise radiation in the low frequency range. The good results of the very light MR foam at medium and low frequencies at the aluminum plate cannot be derived from a high dynamic Young's modulus or damping ratio. It is supposed to be the result of the higher thickness of the probe (40 mm instead of 20 mm).

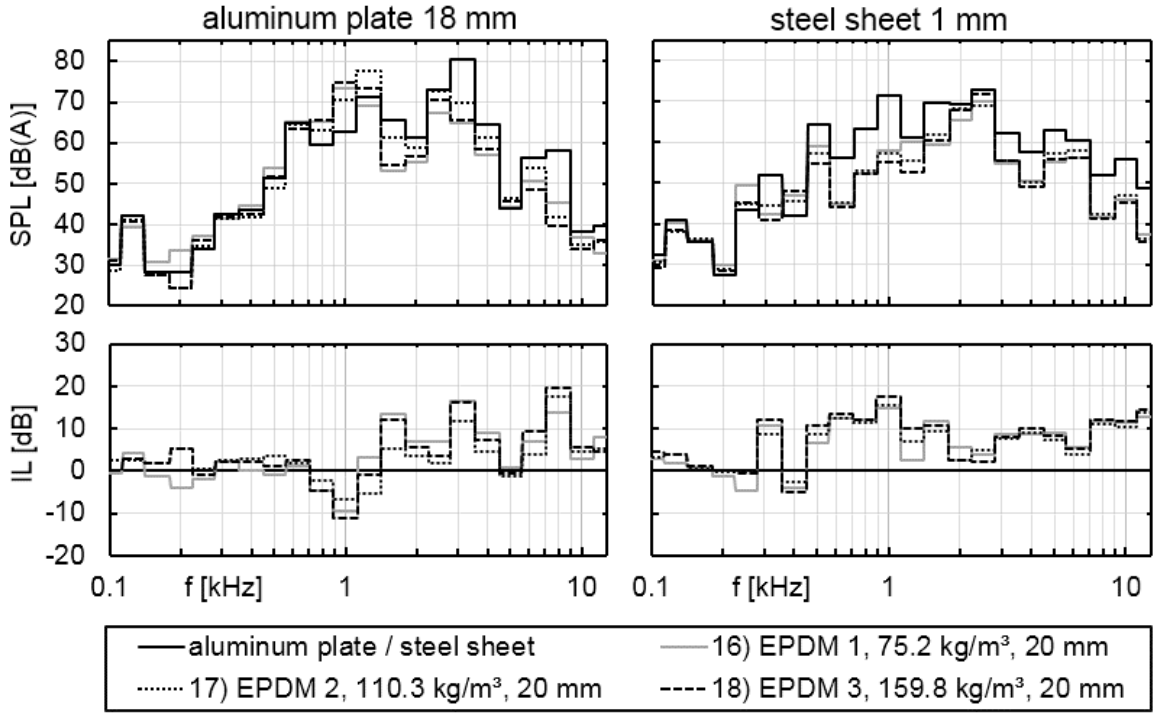

Figure 11: Sound pressure level and insertion loss of EPDM foams of different density

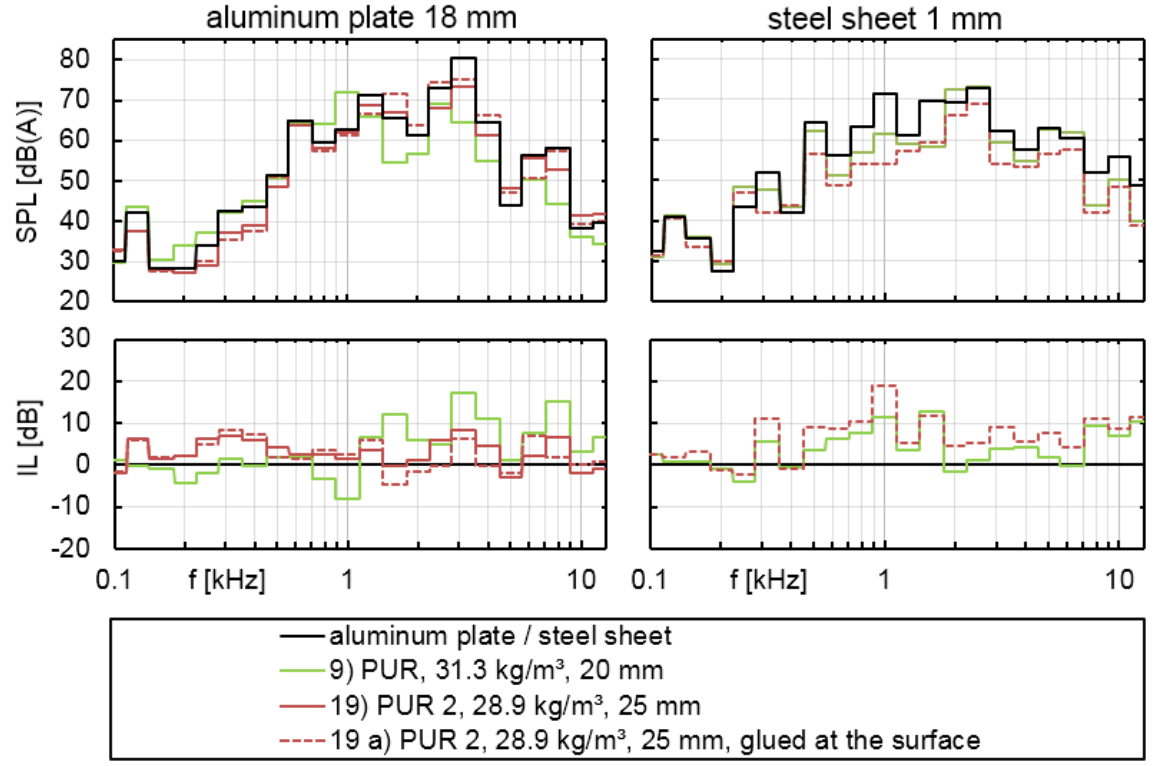

Figure 12: Sound pressure level and insertion loss IL of PUR foams with different mounting conditions

In Figure 11, as well as in Figure 8 and Figure 9, an increase of the density improves the noise reduction at the steel sheet below 1 kHz. Above that frequency, lighter and softer foams show better effects. In contrast, a higher density in the EPDM materials on the aluminum plate leads to an improvement of the damping behavior at the dominating octave bands above 1 kHz.

For the comparison with the simulations presented in the next section another PUR foam ("PUR 2") was examined experimentally, whose Biot parameters are known. This additional material allows a modeling with the complex approach described in the first section. To ensure the comparability of the finite element model and the experimental setup the foam was not only fixed with the frame to the aluminum plate but additionally with double-sided tape. So, a planar coupling between plate and foam was ensured and later adopted for the simulation. Figure 12 shows the acoustic effect of the foam for its two different mounting configurations on the aluminum plate in comparison to the effect of the PUR foam examined above. The results for the surface glued PUR 2 foam are used as a reference for the numerical investigations.

4 Numerical investigation

Two numerical models of the aluminum plate used in the experimental investigation above were examined. The models differ in their complexity. For all numerical simulations in this paper the Finite Element Method (FEM) is used. The simpler model (Variant 1) is shown in Figure 13, the more complex (Variant 2) in Figure 14. Variant 1 includes the rectangular aluminum plate and the material sample. All boundary conditions are applied directly on the aluminum plate (see the red dots in Figure 13). In each highlighted node all three degrees of freedom (displacement) are pinned. The excitation load is also applied directly to the aluminum plate, in the middle of the backside. In the simple model exclusively hexahedral elements with quadratic shape functions are used.

The results of the simple model with constant and frequency-dependent stiffness and damping can be seen exemplarily for one investigated damping material in Figure 18 in comparison to the measurement in the acoustic test bench. The results are shown in terms of insertion loss curves as the difference of the calculated sound power of the aluminum plate with and without applied damping material. Obviously, the simple model is not sufficient to represent the real setup. For this reason a more complex simulation model was built (Variant 2), which is displayed in Figure 14. The Variant 2 additionally contains the steel hooks on which the whole system is suspended as well as a part of the connection rod to the shaker by which the load is applied and which represents an additional boundary condition. Due to the more complex geometry this model requires also tetrahedral elements for modeling, for which quadratic shape functions were used as well. To ensure the model's quality, a validation is conducted.

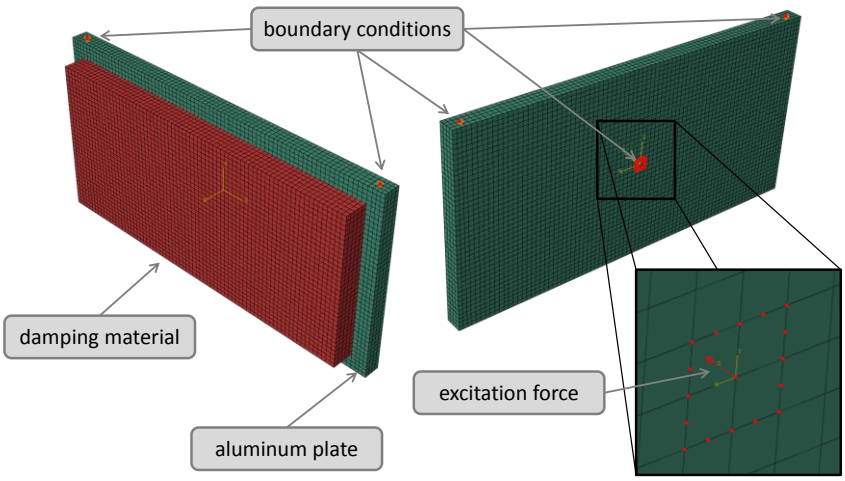

Figure 13: Simple numerical model (Variant 1) of the aluminum plate in the acoustic test bench

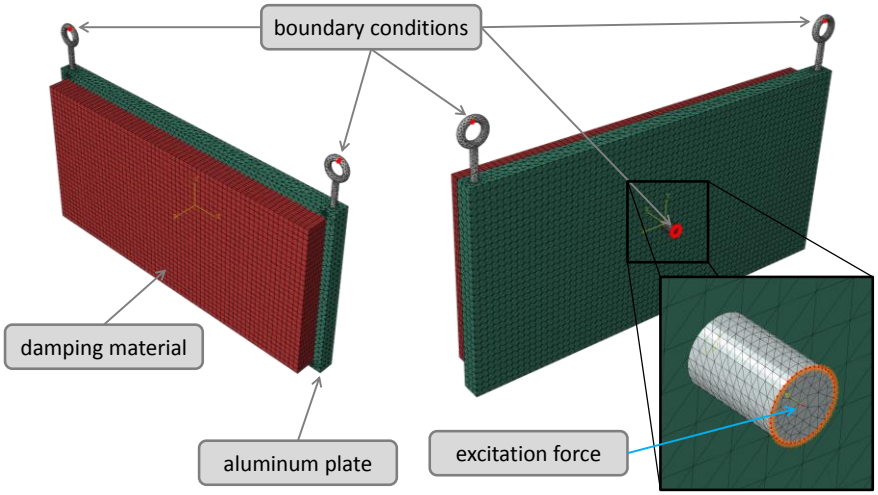

Figure 14: Complex numerical model (Variant 2) of the aluminum plate in the acoustic test bench

For this purpose, a one dimensional Laser-Scanning-Doppler-Vibrometer was used to measure the vibration behavior of the plate without damping material. The aim was to validate the model itself including all loads and boundary conditions, without additional uncertainties caused by the damping material. The experimental setup is shown in Figure 15 both as schematic sketch and as a photograph.

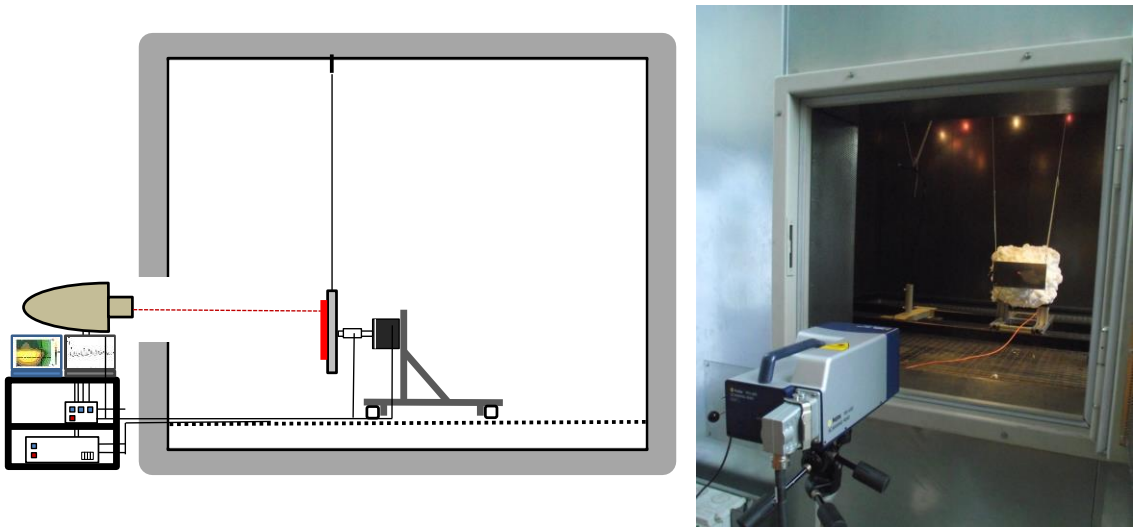

Figure 15: Experimental vibration analysis on the acoustic test bench via Laser-Scanning-Vibrometer

The comparison of the experimental and the numerical vibration analysis of the aluminum plate without additional damping material in Figure 16 makes clear that the complex model (Variant 2) can capture the vibration behavior of the acoustic test bench very well. In Figure 16, three arbitrary eigenfrequencies and their corresponding eigenmodes are shown. It has to be noted that even in the high frequency regime the model prediction is close to the measured data, even if the difference in the eigenfrequencies becomes larger. In contrast, the agreement of the eigenmodes is very good in the whole frequency range.

For the calculation of the radiated sound power of the different configurations a vibroacoustic simulation was necessary. For this purpose, the vibrating structure is fully coupled to a fluid domain. The surrounding fluid volume was modeled as a half sphere and meshed with quadratic tetrahedral elements, which only have the acoustic pressure as a single degree of freedom. The size of the elements has to ensure that all wavelengths of interest can be approximated with sufficient accuracy. The resulting mesh is displayed in Figure 17. To avoid reflections on the borders of the discretized region and, thus, to fulfill the free field radiation condition, an absorbing boundary condition was applied on the outer surface of the fluid volume.

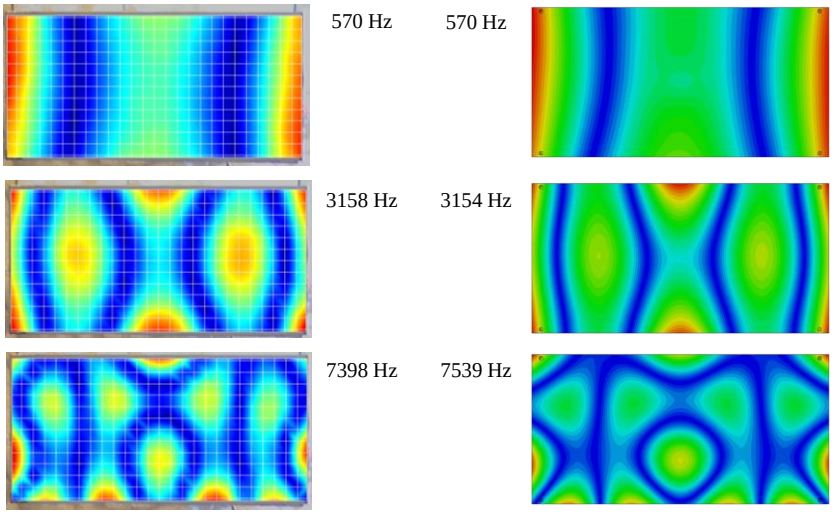

Figure 16: Comparison of the experimental (left) and the numerical (right) vibration analysis of the aluminum plate without additional damping material

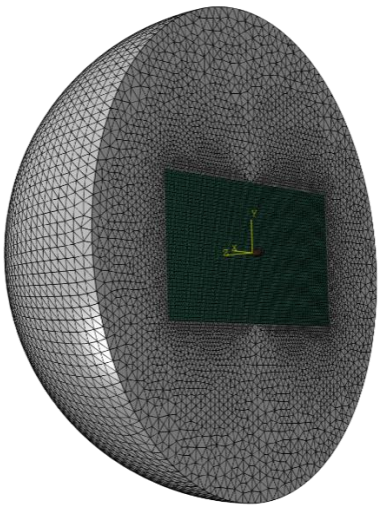

Figure 17: Discretization of the fluid domain in the surrounding of the emitting structure

In Figure 18 the calculated insertion loss (IL) curves of the two different models are contrasted to the experimental results of the PUR 2 foam glued to the surface of the aluminum plate and the steel sheet. The experimental results are shown in Figure 12. As expected, it can be seen that the more complex model of the test configuration leads to results that are closer to the experimental ones. Especially the conspicuous peaks in the IL curves calculated with the simple model are not observable in the experimental results. For the stiff aluminum plate a frequency-dependent modeling of the damping and the elasticity delivers more accurate results than a classical model with constant material parameters. This observation can be made for both the simple model (Variant 1) and the complex model (Variant 2).

Nevertheless, even the prediction quality of the complex model with frequency-dependent material parameters is not yet satisfactory in comparison with the measured data. Consequently, further investigations and improvements have to be made. The calculated IL curve of the corresponding poroelastic material formulation is given with the yellow graph in the upper diagram of Figure 18. For this calculation the JCA-approach was applied. The poroelastic model also shows some peaks that are not visible in the measurement results, and the overall agreement is not sufficient either. At least, it can be stated that the presented approach which uses frequency-dependent determined stiffness and damping values has for the given test case an accuracy that is comparable to the common Biot model.

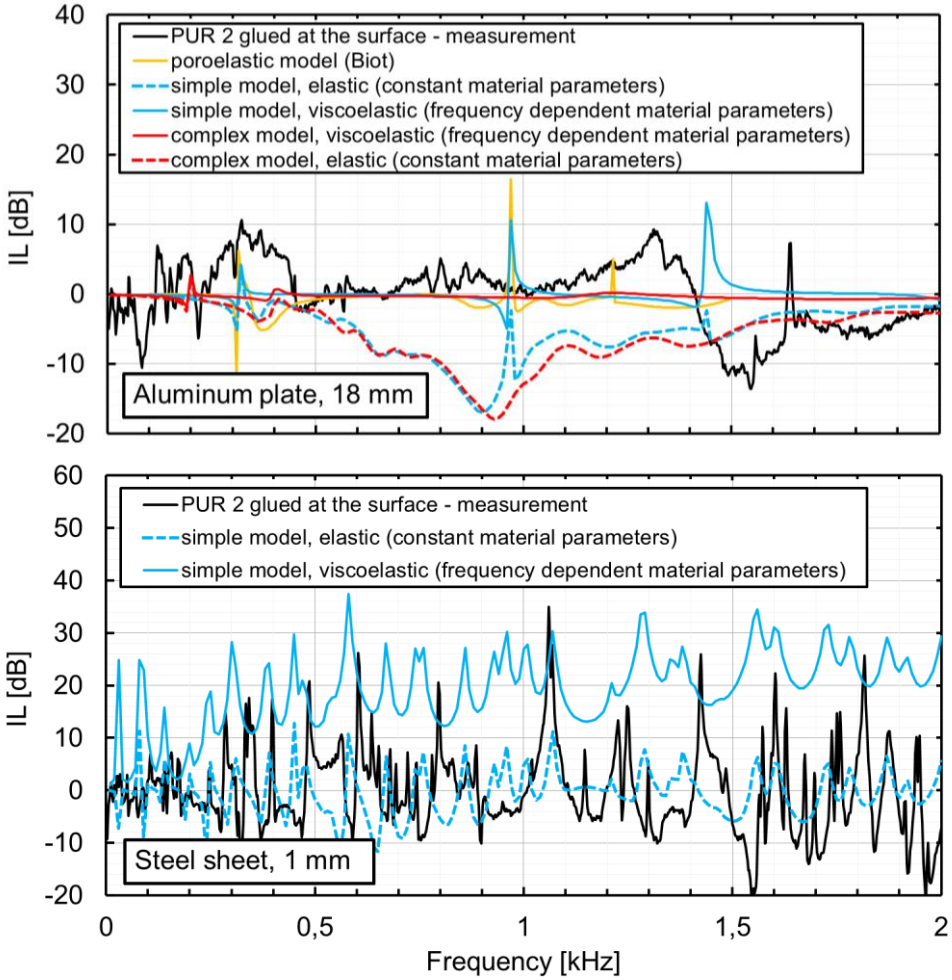

Figure 18: Calculated insertion loss (IL) compared with experimental data from the 18 mm aluminum plate and the 1 mm steel sheet. The yellow curve represents JCA-calculation for this application case; the red curves show the results of Variant 2 of the aluminum plate model.

In contrast, it becomes clear that the usage of frequency-dependent material parameters to represent a viscoelastic material behavior overestimates the IL in the case of the thin steel plate. For this example, the constant material parameters show a better agreement with the experimental results. However, it has to be noted again that all tested simulation approaches lead to insufficient results for the examined test cases. Possible reasons for this have been already mentioned in the text above. Other causes may emerge in further studies that will focus both on the experimental determination of dynamic material properties on the one hand, and on an adequate, simplified and generalizable damping modeling for acoustical predictions on the other hand.

5 Summary and outlook

The aim of this study was to examine a simplified modeling method for poroelastic materials that avoids the experimental and simulative efforts of the complex modeling of such materials based on the Biot formulation. The proposed method considers the frequency dependency of the stiffness and damping as sufficient parameters to numerically predict the dissipation behavior of poroelastic materials in different application cases. This can be derived without knowledge of the open porosity, the viscous and thermal characteristic length, the tortuosity and other specific properties of poroelastic materials. The effects of these poro-mechanical parameters, so the made assumption, can effectively be measured and summarized by the frequency-dependent complex Young's modulus. For this purpose different experimental setups were constructed and tested in advance. The best variant was used in this investigation to measure the

parameters for 19 different material samples. These measurements were reliable only up to a frequency of 2 kHz. The acoustical effects of the tested materials on the noise radiation of a stiff aluminum plate and a more flexible steel sheet were investigated in an anechoic chamber as well.

The test setup of the acoustical experiment was approximated by two finite element models that differed in their complexity. The accuracy of the structural models was verified by laser vibrometer measurements of the aluminum plate in the acoustic test setup. The results of the complex model showed the best agreement with the vibration characteristics of the test setup.

All calculated insertion losses differed significantly from the experimental results. The best fitting was obtained with the frequency-dependent modeling in the complex model of the aluminum plate. For the steel sheet, the simple solution with frequency independent material parameters reached the best agreement while the frequency-dependent overestimated the IL of the plastic foam.

The results of this study show that the proposed simplified approach with frequency-dependent stiffness and damping values is able to approximate the results of an advanced poroelastic formulation and deliver better results than a simple elastic formulation, depending on the application case. To obtain a higher agreement and achieve a better prediction further investigations are necessary. On the one hand, the experimental measurement of the material parameters should be extended to higher frequencies, and influences of the experiment setup on the measured parameters have to be identified to be reduced, if existent. On the other hand, the test setup could be preliminary simplified to gain more knowledge and accuracy in modeling the damping behavior of the porous materials. The poroelastic material could be regarded in its structural behavior alone without acoustic coupling and calculation of the surrounding fluid domain. The experimental reference would be Laser-Scanning-Vibrometer measurements of the vibrating structure with and without poroelastic material. Additionally, a reverse optimization) could deliver the best fitting dynamic Young's modulus and damping coefficient curves. Their comparison with real measured data would improve the knowledge of the physical appropriateness of the approach.

6 References

[1] BIOT, M.A.: Theory of Propagation of Elastic Waves in a Fluid-Saturated Porous Solid. I. Low-Frequency Range. The Journal of the Acoustical Society of America, Vol. 28 (1956) Nr. 2, pp. 168–178.

[2] BIOT, M.A.: Theory of Propagation of Elastic Waves in a Fluid-Saturated Porous Solid. II. Higher Frequency Range. The Journal of the Acoustical Society of America, Vol. 28 (1956) Nr. 2, pp. 179–191.

[3] ALLARD, J.-F.; DAIGLE, G.: Propagation of Sound in Porous Media. Modeling Sound Absorbing Materials. The Journal of the Acoustical Society of America, Vol. 95 (1994) Nr. 5, pp. 2785.

[4] JOHNSON, D.L.; KOPLIK, J.; DASHEN, R.: Theory of dynamic permeability and tortuosity in fluid-saturated porous media. Journal of Fluid Mechanics, Vol. 176 (1987) Nr. 1, p. 379.

[5] CHAMPOUX, Y.; ALLARD, J.-F.: Dynamic tortuosity and bulk modulus in air-saturated porous media. Journal of Applied Physics, Vol. 70 (1991) Nr. 4, pp. 1975–1979.

[6] JAOUEN, L.; RENAULT, A.; DEVERGE, M.: Elastic and damping characterizations of acoustical porous materials. Available experimental methods and applications to a melamine foam. Applied Acoustics, Vol. 69 (2008) Nr. 12, pp. 1129–1140.

[7] SALISSOU, Y.; PANNETON, R.: Pressure/mass method to measure open porosity of porous solids. Journal of Applied Physics, Vol. 101 (2007) Nr. 12, p. 124913.

[8] ATALLA, Y.; PANNETON, R.: Inverse acoustical characterization of open cell porous media using impedance tube measurements. Canadian Acoustics, Vol. 33 (2005) Nr. 1, pp. 11–24.

[9] POMPOLI, F., et al.: How reproducible is the acoustical characterization of porous media? The Journal of the Acoustical Society of America, Vol. 141 (2017) Nr. 2, p. 945.

[10] VAN DER KELEN, C., et al.: On the influence of frequency-dependent elastic properties in vibro-acoustic modeling of porous materials under structural excitation. Journal of Sound and Vibration, Vol. 333 (2014) Nr. 24, pp. 6560–6571.

[11] DAZEL, O., et al.: Expressions of dissipated powers and stored energies in poroelastic media modeled by {u,U} and {u,P} formulations. The Journal of the Acoustical Society of America, Vol. 123 (2008) Nr. 4, p. 2054–2063.

[12] SPANNAN L., et al.: On the characterization of damping materials for acoustic simulations, in preparation, (2018).